Predicting the Solar Thermochemical Water Splitting Ability and Reaction Mechanism of Metal Oxides: a Case Study of the Hercynite Family of Water Splitting Cycles

Christopher L. Muhich[a], Brian D. Ehrhart[a], Vanessa A. Witte[a], Samantha Miller[a], Eric N. Coker[b], Charles B. Musgrave[a,c*], Alan W. Weimer[a*]

[a]Department of Chemical and Biological Engineering, University of Colorado, Boulder, Colorado 80309, USA

[b]Sandia National Laboratories, Albuquerque, New Mexico 87123, USA

[c]Department of Chemistry and Biochemistry, University of Colorado, Boulder, Colorado 80309, USA

[*]Corresponding Author: Email addresses: Alan.Weimer@colorado.edu and Charles.Musgrave@colorado.edu

Supplementary Information

SI.1 Computational Methods

We performed plane wave periodic boundary condition DFT simulations using the Vienna Ab initio Simulation Program (VASP).[28,29] Calculations employed the Perdew-Burke-Ernzerhof (PBE) generalized gradient approximation (GGA) exchange and correlation functional[30] coupled with projector augmented wave (PAW) pseudopotentials.[31] PAWs described the hydrogen 1s; oxygen 2s and 2p; cobalt and iron 4s and 3d; and aluminum 3s and 3p electrons explicitly. All calculations utilized a 500 eV cut-off energy based on a cut-off energy study conducted in the range of 450 to 550 eV. A 500 eV cut off energy was determined to be sufficiently accurate, as demonstrated by the small 0.29 kJ/mol difference in energy for a $CoAl_2O_4$ 112 atom supercell described using plane waves with 500 and 550 eV cutoff energies. We conducted calculations using a Γ-point centered 2×2×2 Monkhorst-Pack k-point mesh. A k-point study determined that there was only a 0.96 kJ/mol difference between using the 2×2×2 Monkhorst-Pack k-point mesh

expansion and the more computationally expensive 4×4×4 mesh. This confirmed the effectiveness of only using the Γ-point k-point.

Bader charge analysis was conducted using software from the Henkelman group.[32,33] A Hubbard term[34] of U_{eff} = 3 and 2 eV on the Fe and Co d-electrons, respectively, was included in the calculations because the GGA functional alone does not adequately describe the electron correlation in these systems. The Hubbard correction attempts to describe electron correlation more accurately by imposing an energy penalty for partial electron occupation of a specific orbital type on a given element. We utilized a Hubbard correction of 3 and 2 eV for U_{eff} because it has been shown to accurately predict the electronic structures of Fe- and Co-based spinels.[35] The spinel supercell is composed of eight (2×2×2) primitive unit cells, as shown in Figure SI1. We chose a random distribution of cations for inverse spinels where multiple elements reside on the A site. The calculated relative energies of the inverse and normal configurations of the spinels considered in this work are reported in Table SI 1. Several spin configurations were attempted for each spinel, including ferromagnetic and multiple anti-ferromagnetic structures. The relative energies of the various spin configurations are also shown in Table SI 1. The lowest energy spin configurations were used in calculating reaction energies.

Geometric relaxations were converged to an energy difference of less than 0.1 kJ/mol between relaxation steps. The supercell geometry and the internal positions of the cations were allowed to relax from their positions in the defect-free cell when O-vacancies were introduced. Reaction energies were calculated using Equations SI1 and SI2 for stoichiometric and O-vacancy formation based reactions, respectively.

$$E_{stoich} = E_{prod} + n\mu_O - \sum_i E_{react,i} \quad \text{(SI1)}$$

$$E_{O-vac} = E_{vac} + \mu_O - E_{cell} \quad \text{(SI2)}$$

In Equations SI1 and SI2, E_{stoich} is the reaction energy of the stoichiometric reaction, E_{prod} is the energy of product material, n is the number of O atoms released by the reaction, μ_o is the chemical potential of an O atom, which is taken to be the calculated energy of splitting water (i.e. $\mu_o = \Delta H_{(H2O)\ exp} - E_{(H2O)DFT} + E_{(H2)DFT}$), $E_{react,i}$ is the energy of the metal oxide i involved in the reaction, $E_{O\text{-}vac}$ is the O-vacancy formation energy, E_{vac} is the energy of the supercell containing an O-vacancy, and E_{cell} is the energy of the perfect material, modeled as the energy of a supercell of the material that does not contain an O vacancy.

SI.2 Materials Preparation

Doped-hercynite was produced by both atomic layer deposition (ALD) and a modified Pechini (citrate gel) method.[37] All ALD depositions were performed in a vibrating fluidized bed reactor described elsewhere.[38] Films of Al_2O_3 were deposited on Cavilink™ polymer supports by ALD using trimethyl aluminum (Sigma Aldrich 97% pure) and in-house DI water. The polymer was removed via combustion in air and $CoFe_2O_4$ was subsequently deposited on the alumina skeleton via ALD using cobaltocene (Strem Chemicals >98% metal purity), ferrocene (Strem Chemicals >99% metal purity), and O_2 (AirGas UHP) as precursors. More detailed descriptions of the materials preparation have been described elsewhere.[24,39] This method produced material that is 19.8% $CoFe_2O_4$ with the balance being alumina as determined by inductively coupled plasma optical emission spectrometry (ICP-OES). This results in a material that is 47% active on a mass basis where the active material is defined as the percent of the total material which is capable of forming $Co_xFe_{1-x}Al_2O_4$. The ALD produced material was used in the HT-XRD and SEM/EDS experiments reported herein.

Citrate gel fabrication was used to produce $FeAl_2O_4$ and $(Co_{0.4}Fe_{0.6})_{1.2}Al_{1.8}O_4$ for use in the H_2O splitting stagnation flow reactor experiments. In the citrate gel method, metal nitrate salts, $Fe(NO_3)_3 \cdot 9H_2O$, $Al(NO_3)_3 \cdot 9H_2O$, or $Co(NO_3)_2 \cdot 6H_2O$ (all >98% pure from Alpha Aesar), were dissolved in ethylene glycol (Fisher Scientific reagent grade) in a 1:60 total metal ion to glycol molar ratio; citric acid (Citric Acid monohydrate from Fisher Scientific) was subsequently added to the ethylene glycol in a 1:4 citric acid:ethylene glycol ratio. The solution was heated to ~120°C, whereupon it formed a metal cation containing polymer and solidified. The organic content of solid was combusted away in an air filled furnace at 450°C for 6 hours and the resulting oxides were calcined in air at 850°C for 46 hours. ICP-OES determined that $FeAl_2O_4$ and $(Co_{0.4}Fe_{0.6})_{1.2}Al_{1.8}O_4$ had compositions of $Fe_{1.19}Al_{1.81}O_4$ and ($Co_{0.41}Fe_{0.59}Al_2O_4$ + 0.105 Al_2O_3), respectively. A small amount of Si was also detected in each of the samples; however, similar quantities of Si were also detected in commercial ≥99% pure samples, therefore we attribute the detected Si to the ICP-OES sample preparation method, which included an HF digest. $CoAl_2O_4$ (≥99% purity) was purchased from Sigma Aldrich.

SI.3 Experimental Methods

We used three different experimental approaches to validate the computational results: H_2O splitting experiments carried out in a stagnation flow reactor, high temperature XRD analysis, and SEM/EDS analysis.

SI.3.1 Method for Determining H_2 Production Capacity of Aluminates

We determined the H_2 production capacity of the doped-hercynite material and the new $CoAl_2O_4$ and $FeAl_2O_4$ materials in a stagnation flow reactor (SFR). Roughly 0.1 g of material was loosely placed as a thin layer in an alumina boat and placed in an in-house built stagnation

flow reactor. The stagnation flow reactor consists of two alumina tubes configured to produce an annulus where the exit of the inner tube creates a stagnation zone over the surface of the reacting material.[7,40] The SFR was heated with an electric furnace and steam was generated using an RSIRC RainMaker® steam delivery system. An in-house programmed LabView code controlled the system and recorded system data such as up-stream and down-stream pressures, reactor temperature, and gas flow rates.

Sweep and reactant gasses entered the SFR through the center tube, flowed over the reactive material, and then exited through the annulus. After exiting the reactor, the gas stream passed through a Drierite (anhydrous $CaSO_4$) desiccant column to remove any unreacted steam. The removal of excess steam prevents the dissociation of water in the mass spectrometer which convolutes the H_2 production signals and thus aids in accurate O_2 measurements. A portion of the dried gas flowed to a Stanford Research QMS200 mass spectrometer with a capillary sampling port, while the majority passed through an Advanced Microsystem Instruments Inc. 2001-RS O_2 oxygen analyzer. The hydrogen (H_2) generation was measured using the mass spectrometer, while O_2 was measured using the O_2 analyzer. The mass spectrometry data were recorded by a stand-alone program written by Stanford Research, while the O_2 analyzer data were recorded by LabView. Both the mass spectrometer and O_2 analyzer were calibrated for H_2 and O_2, respectively, using a calibration gasses and three point calibration curve.

The active materials were allowed to reduce for 60 min at 1500°C and a total pressure of 760 Torr; a 300 sccm flowrate of He swept the generated O_2 out of the reactor. Oxidation occurred for 15 min at 1350°C and at 760 Torr total pressure in a 50% H_2O/50% He environment with a total gas flow rate of 400 sccm. Blank runs with no active material present in the reactor were conducted and the H_2 production from heterolytic water splitting was subtracted from the sample

runs. The $FeAl_2O_4$ and $Co_{0.4}Fe_{0.6}Al_2O_4$ materials were cycled 12 times while the $CoAl_2O_4$ was only cycled 6 times, because no STWS activity was observed. The first six cycles of $FeAl_2O_4$ and $Co_{0.4}Fe_{0.6}Al_2O_4$ are not reported as these cycles are not representative of the long term material behavior due to material calcination and sintering.[41] Average H_2 production capacity confidence intervals are reported for the last six cycles at a 95% confidence level.

SI.3.2 Method for Determining Solid Phases during Doped-Hercynite Driven STWS

We performed high temperature X-ray diffraction (HT-XRD) experiments to determine the solid species present during isothermal doped-hercynite CO_2 splitting. CO_2 was employed as the oxidizing gas instead of water to prevent condensation within the HT-XRD. The XRD patterns were measured using a Scintag PAD X diffractometer (Thermo Electron Inc.; Waltham, MA). The X-rays were produced from a sealed Cu Kα, $\lambda = 0.15406$ nm source and were detected using a Peltier-cooled Ge solid-state detector. The material was seated on a Buehler hot-stage with Pt/Rh heating strip and surround heater, and was contained in a sealed chamber. The X-rays entered through an X-ray-transparent beryllium window. A Centorr TM 1B Oxygen absorber scrubbed O_2 from the He entering the XRD. Oxygen (O_2) and H_2O were removed from the entering CO_2 via an oxygen- and moisture-specific adsorbent purifier bed. An Omega fabricated pyrometer measured the temperature of the sample during experimentation.

Samples of typically 20 – 30 mg material were analyzed as thin layers (ca. 50 – 100 μm) of powder on top of single-crystal <100> 9YSZ platelets (10mm x 10mm x 0.5mm, MTI Corporation). *In situ* HT-XRD experiments were conducted at atmospheric pressure under gas flow rates of 150 sccm. Experiments typically involved purging the reaction chamber with He, then ramping the temperature to 1400 °C which was held for three isothermal reduction and

oxidation cycles. The material was allowed to reduce under He for 50 min, and oxidized under CO_2 for 26 min. Each XRD scan lasted roughly 12 minutes; scans were separated by a 2 minute pause during which the inlet gas was switched between He and CO_2. Scans were separated by a pause of only a few seconds when no change in the inlet gas was made. Diffraction patterns were collected at 40 kV and 30 mA using fixed slits over a 2θ scan range of 20 – 80° at a step-size of 0.04° and a count time of 1 s.

SI.3.3 Method for Determining Phase and Cation Segregation

In addition to XRD analysis, we conducted SEM/EDS analysis to determine if separate spinel and alumina phases form or if a single phase was present after both reduction and oxidation. Additionally, this analysis enabled us to determine if the Fe, Co and Al cations remained well mixed or were segregating within a single phase during cycling. This study used ALD-produced doped-hercynite material which had been precycled over 200 times. Both a reduced and oxidized sample were produced in the SFR, and then analyzed via SEM/EDS. We produced the reduced sample by heating the doped-hercynite material to 1450°C and allowing it to reduce under a 300 sccm He flow for four hours to ensure the material reached equilibrium. The active material was subsequently cooled to room temperature under inert flow. The oxidized sample was produced by first reducing it, as described above, and then oxidizing the reduced material for 4 hours at 1450°C under a CO_2 atmosphere before the sample was cooled to room temperature in the oxidizing environment. Surface material was removed from the samples via focused cation beam (FIB) milling to expose cross sections of bulk material. This was then used to determine the distribution of cations within the material. FIB milling was performed using a dual beam FEI Nova 600 nanolab with a Ga beam for ablation. The milled samples were Au

coated to minimize sample charging. SEM/EDS analysis was conducted using a JEOL JSM-6480LV scanning electron microscope.

SI.4 Justification for excess Al_2O_3 as an inert spectator assumption.

In general, Al_2O_3 is inert to redox processes; however, some Fe dissolves in Al_2O_3 (~5wt% at the relevant temperatures and O_2 partial pressures)[1] and therefore the excess Al_2O_3 could interact in the system actively or not at all. There are four possibilities for how this distinct Al_2O_3 phase behaves. One, there is a stoichiometric reaction between $CoFe_2O_4$ and the Alumina. In this case the excess Al_2O_3 does not participate, and just like any reaction mechanism with excess reagent this does not affect the thermodynamics of the system, but merely drives the reaction further towards completion. However, as shown in the main text, a stoichiometric reaction does not occur and therefore we can eliminate this case from further consideration.

Two, there is an ion exchange reaction between the doped $Co_xFe_{1-x}Al_2O_4$ spinel phase and the Al_2O_3 during reduction and oxidation. Overall, the quantity of Fe exchanged during redox would have to be small as the maximum Fe content in Al_2O_3 is already small (~5%) and the thermodynamic change of the iron solubility in Al_2O_3 does not drastically different over the range of O_2 chemical potentials and temperatures expressed over STWS. Fe or Co and Al ions could exchange in two ways, demonstrated for a pure hercynite. In the first sub-case the Fe content in the Al_2O_3 phase decreases during reduction, as shown in Equation SI.3; in the second sub-case the Fe content in the Al_2O_3 phase increases during reduction, as shown in Equation SI.4.

$$Al_{2-x}Fe_xO_3 + FeAl_2O_4 \rightarrow Al_{2-x+\alpha}Fe_{x-\alpha}O_3 + Fe_{1+\alpha}Al_{2-\alpha}O_4 \quad \text{SI.3}$$

$$Al_{2-x}Fe_xO_3 + FeAl_2O_4 \rightarrow Al_{2-x-\alpha}Fe_{x+\alpha}O_3 + Fe_{1-\alpha}Al_{2+\alpha}O_4 \quad \text{SI.4}$$

If the Fe cations in the Al_2O_3 phases migrate to the spinel phase during reduction (Equation SI.3), the Al_2O_3 lattice contracts while the spinel lattice expands due to the difference in ionic radii. However, we measure spinel contraction via HT-XRD during reduction; therefore the Fe content in the spinel phase should not substantially increase during reduction. If the Fe cations in the spinel phases migrate to the Al_2O_3 phase during reduction (Equation SI.4), the spinel phase should show lattice contraction, which is seen in the HT-XRD. However, this requires the Fe^{2+} ions in the spinel phase to oxidize to Fe^{3+} ions incorporated in the Al_2O_3 phase and Al^{3+} cations to reduce to Al^{2+} as they incorporate into the spinel phase during reduction; oxidation of the Fe species under reducing conditions is illogical. Therefore, we suggest that no major exchange of ions between the spinel and Al_2O_3 phases during redox cycling.

Three, the Fe or Co ions, which are incorporated into Al_2O_3 as dopants, oxidize and reduce within the Al_2O_3 matrix. We have calculated the O-vacancy energy of 529 kJ/mol in ~6.6 wt% Fe in Al_2O_3 (the experimental maximum Fe content in Al_2O_3 is roughly 5.3 wt%) when the O-vacancy neighbors one Fe ion. These high reduction energies suggest that reduction of the Fe or Co reduction within Al_2O_3 is unlikely to occur at anywhere near the same extent as the O-vacancy formation energy in the $FeAl_2O_4$, if at all.

Four, the Al_2O_3 and the any incorporated Fe or Co ions are inert to the process. In this case the second phase does not interact with the doped hercynite and therefore does not affect calculations or analysis. Additionally, the Al_2O_3 behavior seen in the XRD standard and the hercynite sample are very similar. This indicates that the Al_2O_3 in the herycnite sample is inert, as it is in the Pt/ Al_2O_3 standard. Therefore the assumption that excess Al_2O_3 is inert is valid and will be utilized throughout the discussions in this work.

Figures

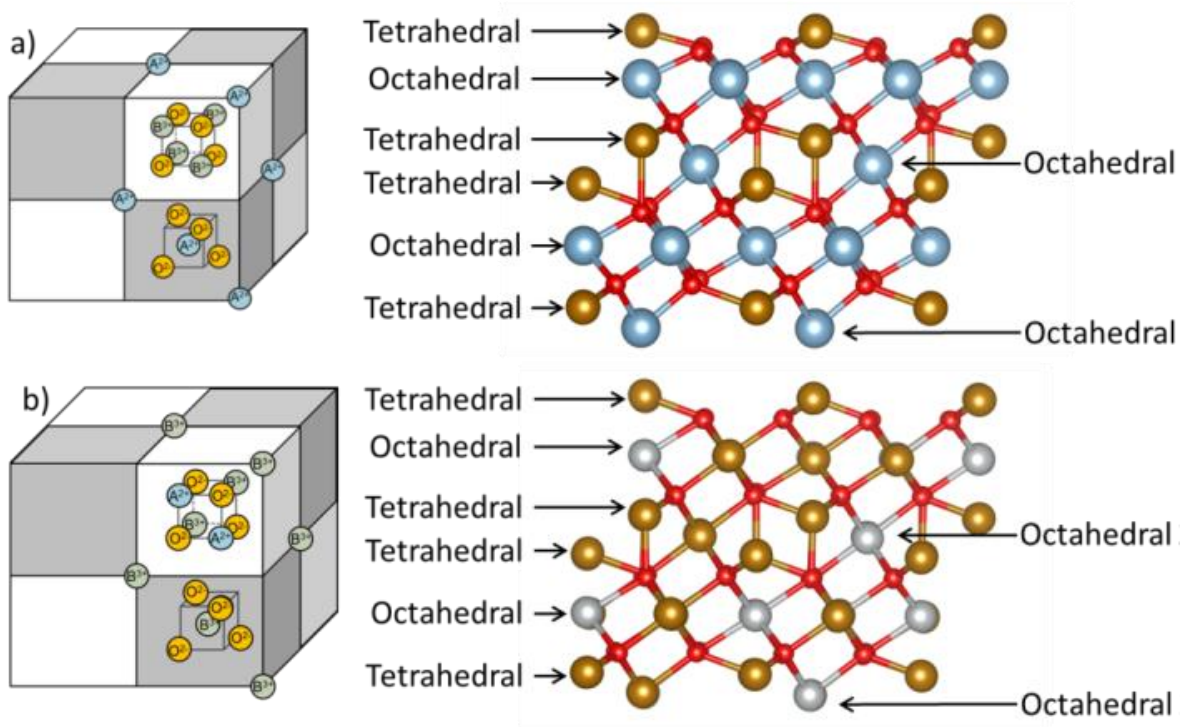

Figure SI1: Representations of the a) normal and b) inverse spinel structures. The figures on the left show the cubic cell representation of the spinel structure where the white cubes represent the octahedral sub-lattice and the gray blocks represent the tetrahedral sub-lattice. The right ball-and-stick models show the spinel supercell containing the 2×2×2 primitive cells used in this work. The small red spheres, medium gold spheres, medium silver spheres, and large blue spheres represent O, Fe, Co, and Al atoms. In the normal spinel, cations with a +2 oxidation state occupy only tetrahedral sites; these are the A^{2+} shown in the left figure and gold Fe^{2+} spheres shown in the right figure. Cations with a +3 oxidation state occupy only octahedral sites; these are the B^{3+} and blue Al^{3+} spheres in the left and right figures, respectively. Conversely, in inverse spinels the cations with a +2 oxidation state occupy only octahedral sites, as shown by A^{2+} and silver Co^{2+} spheres in the left and right figures, respectively. Half of the cations with a +3 oxidation state occupy all of the tetrahedral sites and the remaining half of the octahedral sites, as illustrated by the B^{3+} spheres and gold Fe^{3+} spheres in the left and right representations, respectively.

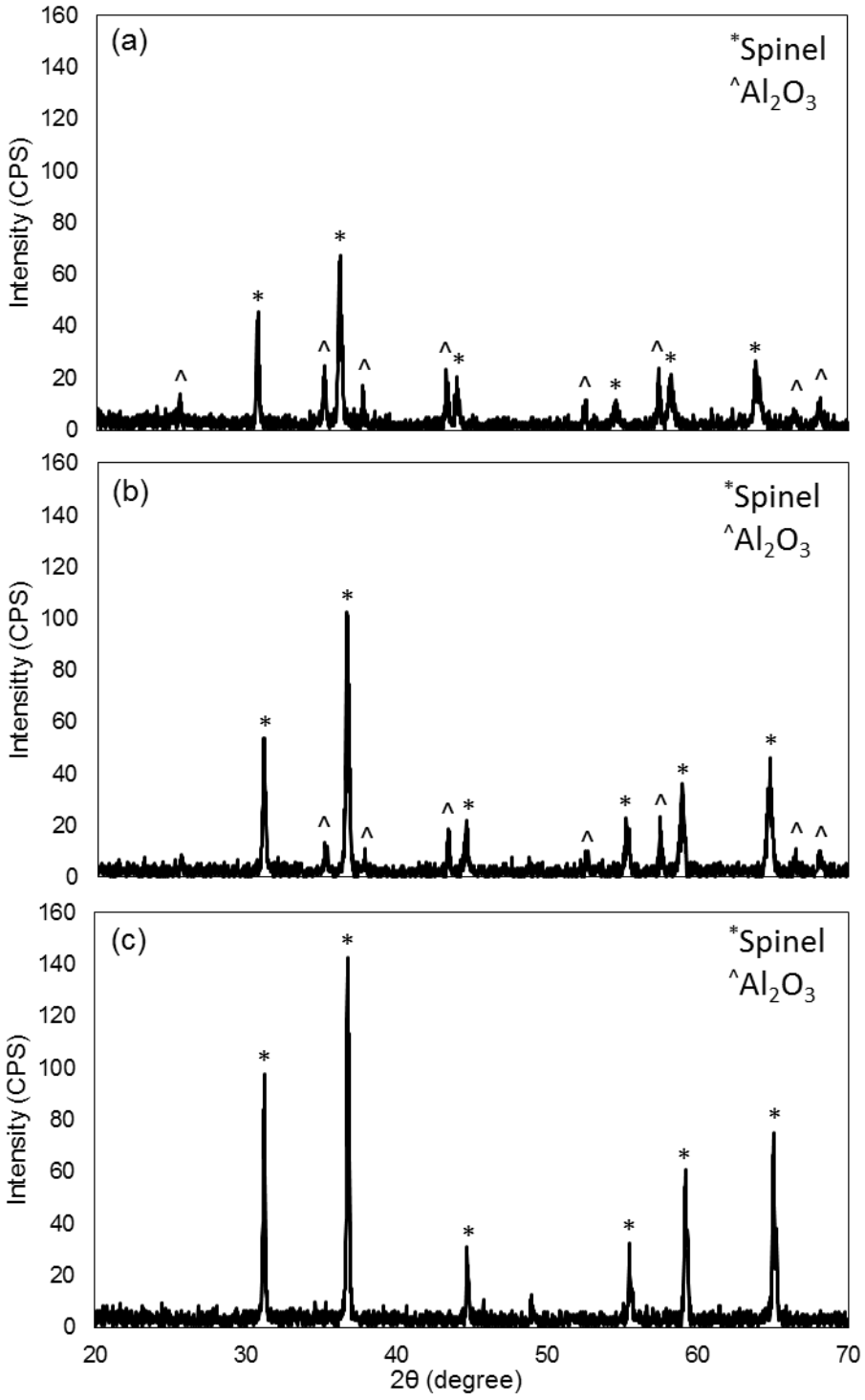

Figure SI 2: XRD spectra for (a) $FeAl_2O_4$, (b) $Co_{0.4}Fe_{0.6}Al_2O_4$, and (c) $CoAl_2O_4$ after redox cycling in stagnation flow reactor. $FeAl_2O_4$ and $Co_{0.4}Fe_{0.6}Al_2O_4$ were fabricated by the Pechini method while $CoAl_2O_4$ was purchased.

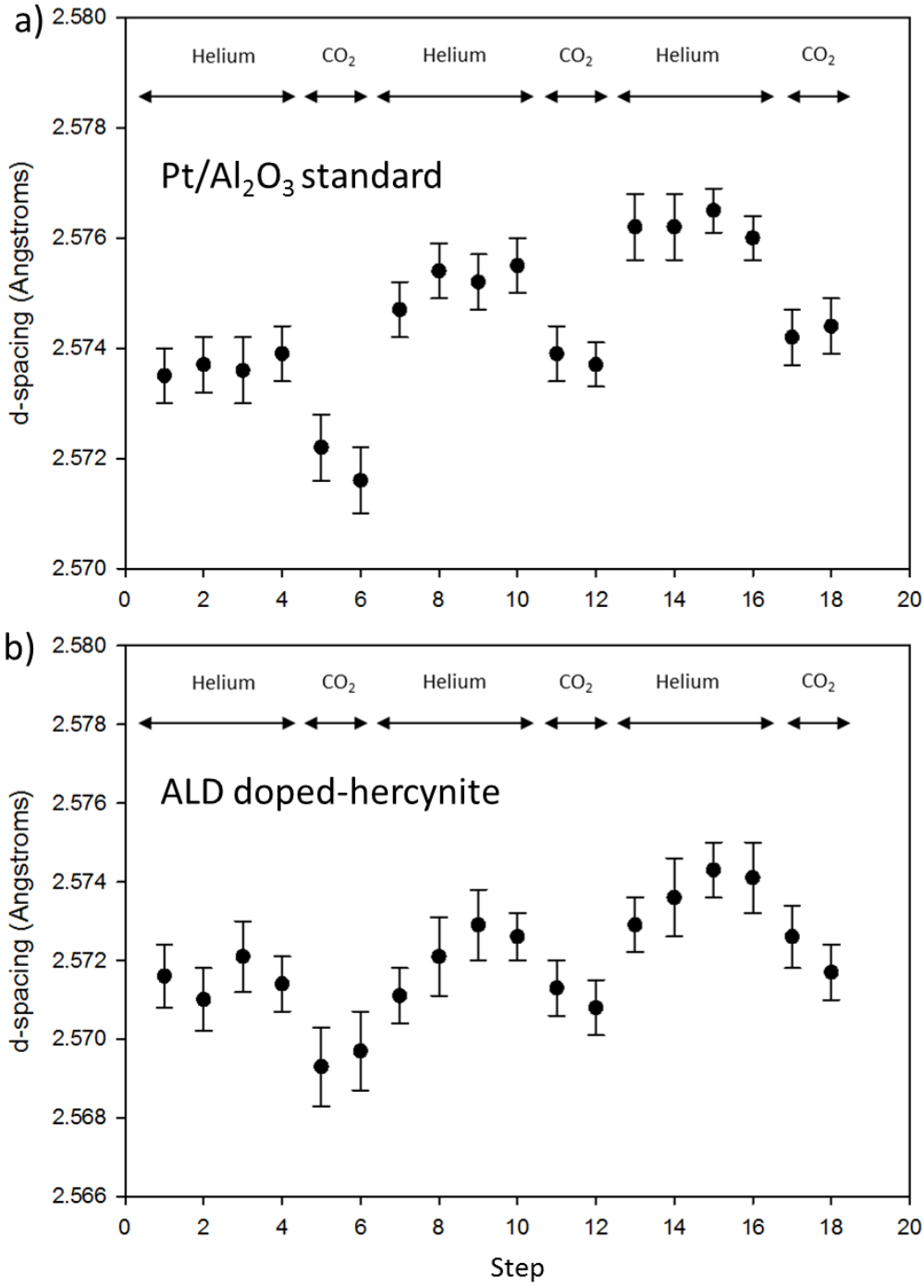

Figure SI 3: The calculated d-space of the 104 Al_2O_3 peak in a) a Pt/Al_2O_3 standard and b) ALD fabricated doped-hercynite material under reducing (He) and oxidizing (CO_2) conditions.

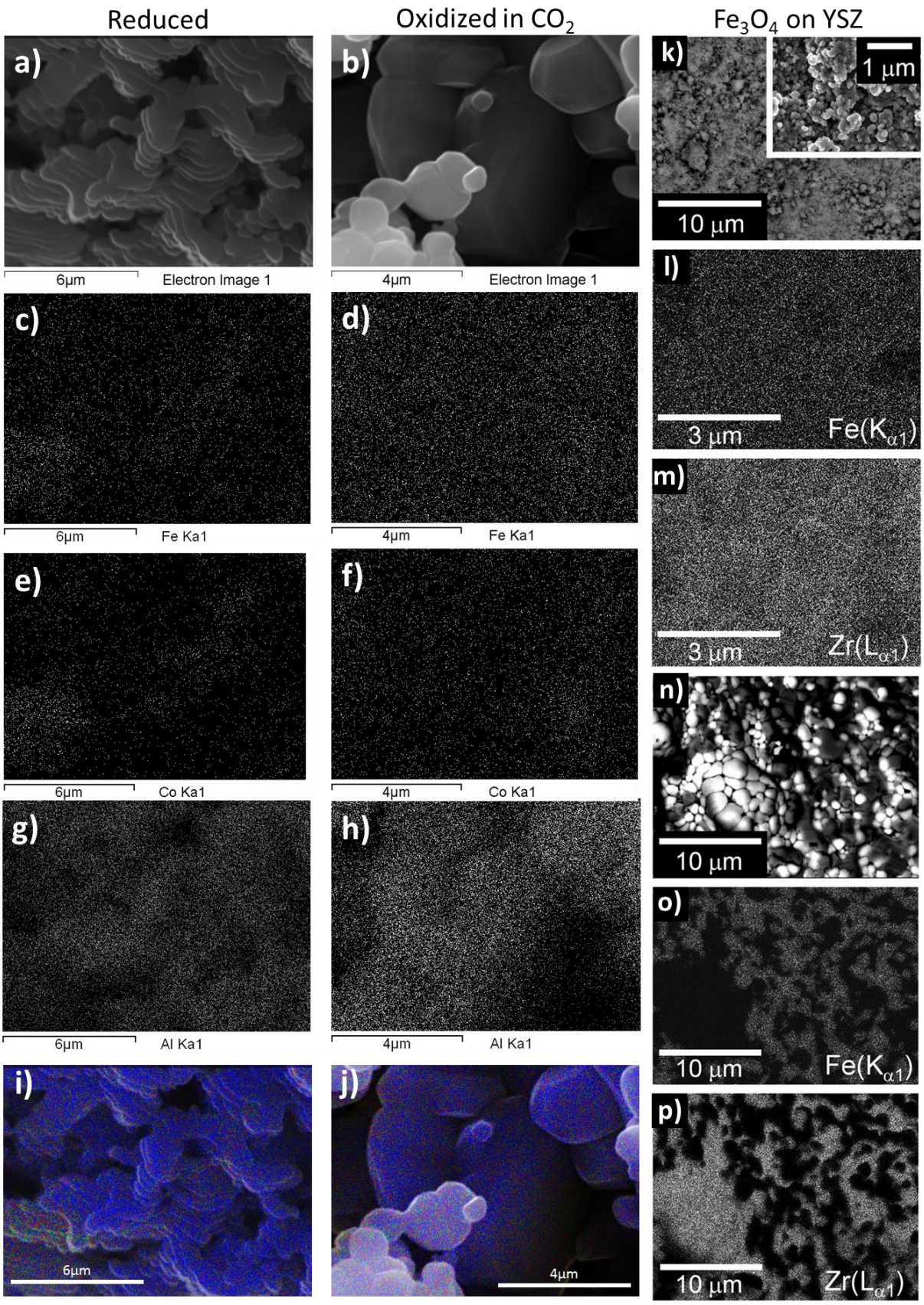
Reduced
Oxidized in CO_2
Fe_3O_4 on YSZ
a)
6µm
Electron Image 1
b)
4µm
Electron Image 1
k)
1 µm
10 µm
l)
3 µm
Fe($K_{\alpha1}$)
c)
6µm
Fe Ka1
d)
4µm
Fe Ka1
m)
3 µm
Zr($L_{\alpha1}$)
e)
6µm
Co Ka1
f)
4µm
Co Ka1
n)
10 µm
g)
6µm
Al Ka1
h)
4µm
Al Ka1
o)
10 µm
Fe($K_{\alpha1}$)
i)
6µm
j)
4µm
p)
10 µm
Zr($L_{\alpha1}$)

Figure SI4: SEM and EDS images of bulk doped-hercynite material exposed by FIB milling after the material is reduced and oxidized in CO_2. The images show: SEM image of the bulk material after a) reduction and b) oxidation; Fe cation EDS map after c) reduction and d) oxidation; Co cation EDS map after e) reduction and f) oxidation; Al cation EDS map after g) reduction and h) oxidation; and an overlay of the EDS cation maps and SEM image after i) reduction and j) oxidation. In i) and j) red, green, and blue dots represent Fe, Co, and Al EDS signals, respectively. k) through p) show SEM/EDS images of Fe_3O_4 on yttria-stabilized zirconia (YSZ) before and after STWS, reproduced from Scheffe *et al*. [47] An SEM of the surface is shown in k) and n) before and after reduction, respectively; l) and o) show an EDS map of Fe before and after reduction, respectively; and m) and p) show an EDS map of Zr before and after reduction, respectively.

Table SI 1: Relative energies in kJ/mol of the spin states for inverse and normal aluminate and ferrite spinels investigated in this work.

Configuration		Co_3O_4	$CoAl_2O_4$	$CoFe_2O_4$	Fe_3O_4	$FeAl_2O_4$
Inverse[a]	All up[c]	135	**0.0**	71	52	**0.0**
	Alternating layers[d]	57	0.7	19	**0.0**	0.3
	Tetrahedral and octahedral[e]	83	N/A	**0.0**	8	N/A
	Other	**0.0**[f]	N/A	N/A	N/A	N/A
Normal[b]	All up[c]	N/A	19	34	N/A	**0**
	Alternating layers[d]		**0**	**0**		54
Inversion energy[g]			**85**	**-14**		**33**
Inversion parameter (x) at 1200 °C[h]			0.02	0.85		0.23

[a]Energy difference, in kJ/mol, between spin configurations of the inverse spinel geometry.
[b]Energy difference, in kJ/mol, between spin configurations of the normal spinel geometry.
[c]All of the electrons for Co and Fe cations are initially set to be spin up.
[d]The electrons of every other layer of Co and/or Fe cations are initially set to alternate spin up and spin down.
[e]The electrons of all tetrahedral cations are initially set to be spin up and the electrons of all octahedral cations are initially set to be spin down.
[f]The electrons of tetrahedral Co cations are initially set to high spin states (μ=3) and the octahedral Co cations are initially set to low spin states (μ=0.1).
[g]The energy difference, in kJ/mol, between the lowest energy inverse structure and normal structure. A positive number indicates that the normal structure is energetically preferred, while a negative number indicates that the inverse structure is preferred.
[h]The inversion parameter was calculated using the method of Wei and Zhang.[36]